

International Journal of Modern Physics A
 © World Scientific Publishing Company

A UNIFIED MODEL OF HIGH-ENERGY ASTROPHYSICAL PHENOMENA

A. DE RÚJULA

*Theory Division, CERN; 1211 Geneva 23, Switzerland
 Physics Department, Boston University, USA*

I outline a unified model of high-energy astrophysics, in which the gamma background radiation, cluster “cooling flows”, gamma-ray bursts, X-ray flashes and cosmic-ray electrons and nuclei of all energies —share a common origin. The mechanism underlying these phenomena is the emission of relativistic “cannonballs” by ordinary supernovae, analogous to the observed ejection of plasmoids by quasars and microquasars. I concentrate on Cosmic Rays: the longest-lasting conundrum in astrophysics. The distribution of Cosmic Rays in the Galaxy, their total “luminosity”, the broken power-law spectra with their observed slopes, the position of the knee(s) and ankle(s), and the alleged variations of composition with energy are all explained in terms of simple and “standard” physics. The model is only lacking a satisfactory theoretical understanding of the “cannon” that emits the cannonballs in catastrophic episodes of accretion onto a compact object.

Keywords: Cosmic Rays; GRBs; XRFs, Gamma Background Radiation, Cooling Flows.

1. Credits

It is not unusual in talks to start with the credits, as in an old film. Many of the ideas I shall discuss have a long pedigree, e.g. that Gamma-Ray Bursts (GRBs) are the main (injection) process for Cosmic Rays¹ (CRs); that GRBs are the main CR (production and acceleration) mechanism², that they are induced by narrow jets emitted by accreting compact stellar objects³; and that their γ -rays are low-energy photons boosted to higher energies by inverse Compton scattering³ (ICS). The concrete realization of these ideas in the “CannonBall” (CB) model is more recent and covers GRBs^{4,5}, X-Ray Flashes⁶ (XRFs), their respective afterglows^{7,8}, the Gamma “Background” Radiation⁹, the CR luminosity of our Galaxy¹⁰, the “Cooling Flows” of galaxy clusters¹¹, and the properties of CRs^{2,12}.

2. Jets in Astrophysics

A look at the sky, or a more modest one at the web, results in the realization that jets are emitted by many astrophysical systems (stars, quasars, microquasars...). One impressive case¹³ is that of the quasar Pictor A, shown in Fig. (1). *Somehow*, the active galactic nucleus of this object is discontinuously spitting *something* that does not appear to expand sideways before it stops and blows up, having by then

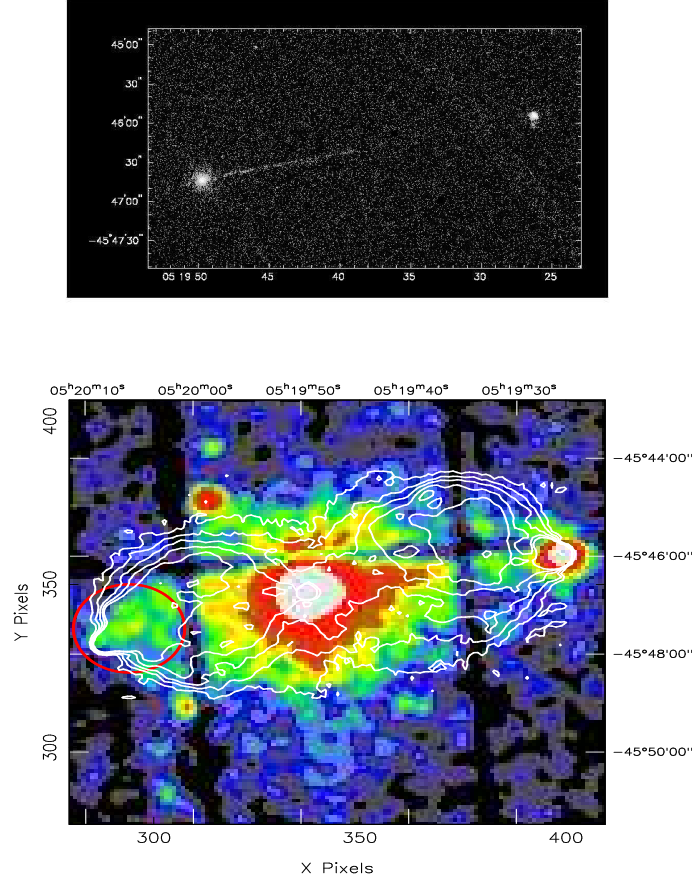


Fig. 1. Upper panel: Chandra X-ray image of the radio galaxy Pictor A: a non-expanding jet emanates from the centre of the galaxy extending across 360 thousand light years towards a hot spot at least 800 thousand light years away from where the jet originates. Lower panel: XMM/p-n image of Pictor A in the 0.2–12 keV energy interval, centred at the position of the leftmost spot in the upper panel, and superimposed on the radio contours from a 1.4 GHz radio VLA map.

travelled for a distance of several times the visible radius of a galaxy such as ours. Many such systems have been observed. They are very relativistic: the Lorentz factors (LFs) $\gamma \equiv E/(mc^2)$ of their ejecta are typically of $\mathcal{O}(10)$. The mechanism responsible for these mighty ejections —suspected to be due to episodes of violent accretion into a very massive black hole— is not understood.

In our galaxy there are “micro-quasars”, in which the central black hole is only a few times more massive than the Sun. The first studied example¹⁴ is the γ -ray source GRS 1915+105. In a non-periodic manner, about once a month, this object emits two oppositely directed *cannonballs*, travelling at $v \sim 0.92c$. As the emission takes place, the X-ray emission —attributed to an unstable accretion disk— tem-

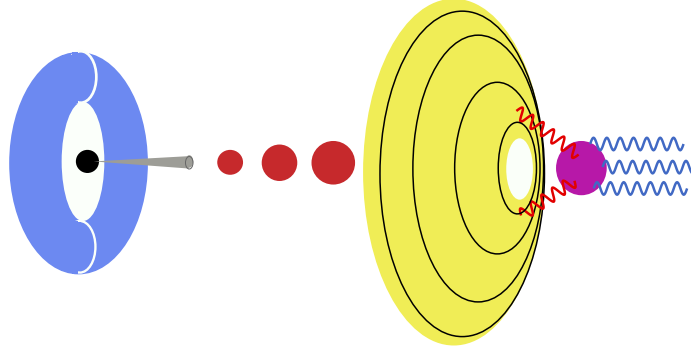


Fig. 2. An “artist’s view” (not to scale) of the CB model of long-duration GRBs. A core-collapse SN results in a compact object and a fast-rotating torus of non-ejected fallen-back material. Matter (not shown) abruptly accreting into the central object produces a narrowly-collimated beam of CBs, of which only some of the “northern” ones are depicted. As these CBs move through the “ambient light” surrounding the star, they Compton up-scatter its photons to GRB energies.

porarily decreases. How part of the accreting material ends up ejected along the system’s axis is not understood. The process reminds one of the blobs emitted upwards as the water closes into the “hole” made by a stone dropped onto its surface. For quasars and μ -quasars, it is only the relativistic, general-relativistic magneto-hydro-dynamic details that remain to be filled in! Atomic lines from many elements have been observed¹⁵ in the CBs of μ -quasar SS 433. Thus, at least in this case, the ejecta are made of ordinary matter, and not of some fancier substance such as e^+e^- pairs.

3. The Cannonball Model

The “cannon” of the CB model is analogous to the ones responsible for the ejecta of quasars and microquasars. *Long-duration* GRBs, for instance, are produced in *ordinary core-collapse* supernovae (SNe) by jets of CBs, made of *ordinary-matter plasma*, and travelling with high Lorentz factors (LFs), $\gamma \sim \mathcal{O}(10^3)$. An accretion disk or torus is hypothesized to be produced around the newly-born compact object, either by stellar material originally close to the surface of the imploding core and left behind by the explosion-generating outgoing shock, or by more distant stellar matter falling back after its passage^{16,4}. A CB is emitted, as observed in microquasars¹⁴, when part of the accretion disk falls abruptly onto the compact object. An artist’s view of the CB model is given in Fig. (2).

Do supernovae emit cannonballs? Up to last year, there was only one case in which the data was good enough to tell: SN1987A, the core-collapse SN in the LMC, whose neutrino emission was detected. Speckle interferometry measurements made 30 and 38 days after the explosion¹⁷ did show two relativistic CBs (one of them “superluminal”), emitted in opposite directions, as shown in Fig. (3).

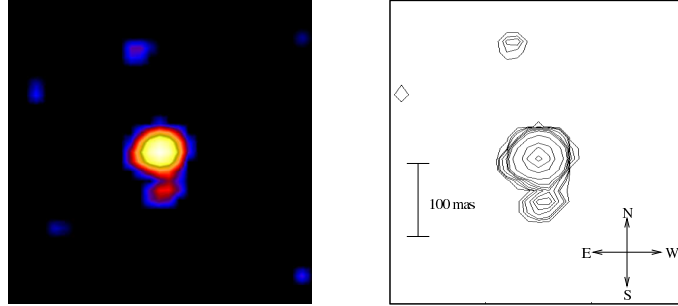


Fig. 3. The two CBs emitted by SN1987A in opposite axial directions. The northern and southern bright spots are compatible with being jets of CBs emitted at the time of the SN explosion and travelling at a velocity equal, within errors, to c . One of the *apparent* velocities is superluminal. The corresponding GRBs were not pointing in our direction, which may have been a blessing.

3.1. *The GRB/SN association*

Are GRBs made by SNe? For long-duration GRBs, the answer is affirmative⁷. The first evidence for a GRB-SN association came from the discovery of SN1998bw¹⁸, at redshift $z = 0.0085$, within the directional error cone²¹ towards GRB 980425. The time of the SN explosion was within -2 to $+0.7$ days of the GRB²². The observations did not fit at all into the framework of the “standard” *fireball* model. This GRB’s fluence was “normal”, but the total “equivalent isotropic” γ -ray energy was $\sim 10^5$ times smaller than that of “classical” GRBs (with $z \sim 1$) transported to $z = 0.0085$. In the CB model the GRB emission is *very* narrowly forward-peaked, with a characteristic opening angle $\sim 1/\gamma \sim 1$ mrad along the opposite jets of CBs. GRBs are detectable if the observer is at an angle $\theta \sim 1/\gamma$ relative to the emission axis. GRB 980425 was seen unusually *far* off-axis, its close location resulting in a “normal” fluence. Its associated SN was seen unusually *close* to its axis of rotational symmetry. Both the GRB and the SN were otherwise “normal”^{4,5,23}.

GRBs have “afterglows” (AGs): they are observable at frequencies ranging from radio to X-rays, for months after their γ -rays are seen. The optical luminosity of a 1998bw-like SN peaks at $\sim 15(1+z)$ days. The SN light competes at that time and frequency with the AG of its GRB, and it is not always easily detectable. In the CB model, it makes sense *to test* whether long-duration GRBs are associated with a “standard torch” SN, akin to SN1998bw, “transported” to their respective redshifts. The test works optimally: *for all cases in which such a SN could be seen, it was seen (with varying degrees of significance) and for all cases in which the SN could not be seen, it was not seen*⁷. The number of cases is now over 30, and the redshift establishing in practice the transition to SN undetectability is $z \sim 1.1$.

Naturally, truly “standard torches” do not exist, but SN1998bw made such a good job at it that it was possible to *predict*^{24,25} the SN contribution to the AG in all recent cases of early detection of the AGs of near-by GRBs (000911, 010921,

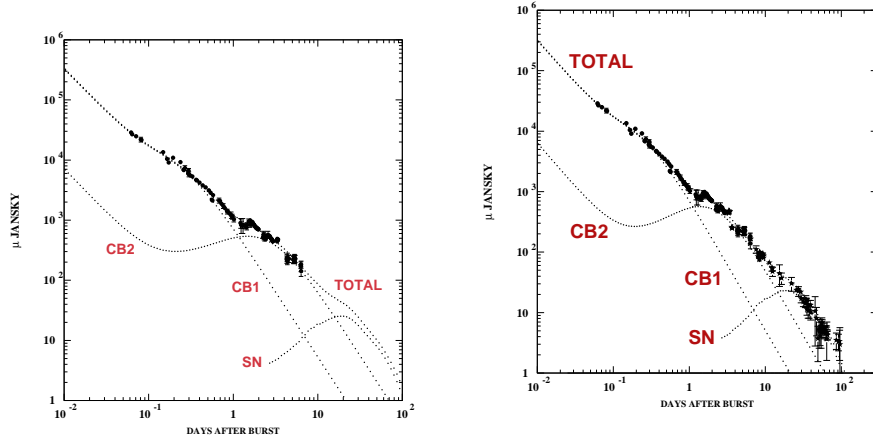


Fig. 4. Left: The R-band AG of GRB 030329, used along with other optical data to predict, in the CB model, the presence of a SN akin to SN1998bw. Right: The subsequent data (the \star symbols) are added.

010405, 012111, 021211 and 030329). Besides the 980425–1998bw pair, the most convincing associations were provided by the spectroscopic discoveries of a SN in the AGs of GRBs 030329²⁶ and 021211²⁷. For GRB 030329, shown in Fig. (4), even the exact date when the SN would be discovered was foretold²⁵.

From a CB-model analysis of GRBs and their AGs^{7,8,24,25} we conclude that GRBs more distant than GRB 980425 are observable with past and current instruments only for $\theta \leq 2\text{--}3$ mrad. With two CB jets per GRB, only a fraction $f \sim 2\pi\theta^2/(4\pi) \sim (2 \text{ to } 4.5) \times 10^{-6}$ of SN-generated GRBs are observable. The local rate of long-duration GRBs, is estimated to be¹⁹ $(2.5 \pm 1.0) \times 10^{-10} \text{ Mpc}^{-1} \text{ yr}^{-1}$ for the current cosmology. The local rate of core-collapse SNe²⁰ is $(7.5 \pm 3.8) \times 10^{-5} \text{ Mpc}^{-1} \text{ yr}^{-1}$. The ratio of these rates, $(3.3 \pm 2.1) \times 10^{-6}$, is consistent with the fraction of observable GRBs. Thus, within the pervasive cosmological factor of a few, the long-GRB/SN association would be 1:1.

3.2. The γ -rays of a GRB and the X-rays of an XRF

Massive stars shed much of their matter in their late life, in the form of stellar “winds”. Even before they die as SNe, they undergo occasional explosions and re-brightenings, that illuminate their semi-transparent “wind-fed” circumstellar material, creating a light eco, or “glory”. The example of the red supergiant V838 Monocerotis is shown in the right panel²⁸ of Fig. (5). As a SN explodes, it also illuminates its surroundings, producing an *ambient light* that permeates the semi-transparent circumburst material, previously ionized by the early extreme UV flash accompanying the explosion, or by the enhanced UV emission that precedes it.

The time structure of GRBs ranges from a single pulse of γ -rays to a complicated superposition of many pulses. A single pulse is generated as a CB coasts through

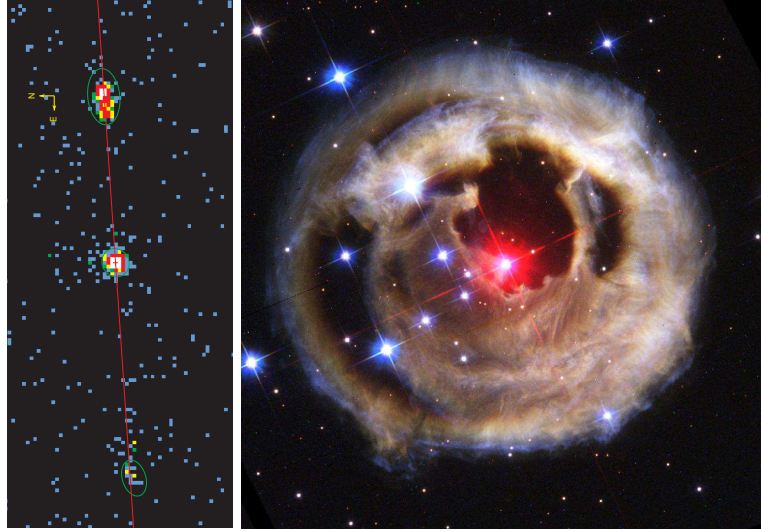


Fig. 5. Left: Two relativistic CBs emitted in opposite directions by the microquasar XTE J1550-564, seen in X-rays. Right: HST picture from 28 October 2002 of the *glory*, or light echo, of the outburst of the red supergiant V838 Monocerotis in early January 2002. The light echo was formed by scattering off dust shells from previous ejections.

the ambient light. The electrons enclosed in the CB Compton up-scatter photons to much higher energies. Each pulse of a GRB corresponds to one CB. The timing sequence of the successive individual pulses (or CBs) reflects the chaotic accretion process and its properties are not predictable, but those of the single pulses are.

To produce, in the CB model, a GRB pulse by ICS on ambient light it suffices to superimpose the two halves^{29,28} of Fig. (5), and to work out in detail^a what the consequences are. These consequences—based exclusively on Compton scattering—are essentially the list of properties of GRBs⁵:

- The narrow distribution of the “peak” or “bend” energies of the GRB spectra³⁰.
- The characteristic peak energy^{30,31} of the γ rays: $E = \mathcal{O}(250)$ keV.
- The duration of the single pulses of GRBs: a median $\Delta t \sim 1/2$ s FWHM.
- The typical (spherical equivalent) number of photons per pulse, $N_\gamma \sim 10^{59}$ on average, which, combined with the characteristic γ energy, yields the average total (spherical equivalent) fluence of a GRB pulse: $\sim 10^{53}$ erg.
- The general *FRED* pulse-shape: a very “fast rise” followed by a fast decay $N(t) \propto 1/t^2$, inaccurately called “exponential decay”.
- The γ -ray energy distribution, $dN/dE \sim E^{-\alpha}$, with, on average, $\alpha \sim 1$ exponentially evolving into $\alpha \sim 2.1$ and generally well fitted³² by the “Band function”.

^aThe “windy” material is assumed to be less dense than average in the “polar” directions.

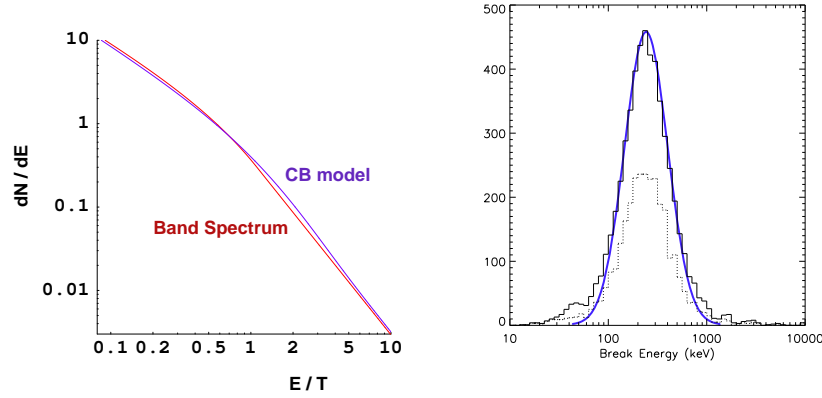


Fig. 6. The GRB spectra: dN/dE . One is the prediction of the CB model. The other is the successful phenomenological Band spectrum; T stands for the “peak” energy in the Band’s case. The agreement is rather satisfying. The peak energy, or E_p distribution of an ensemble of BATSE GRBs. The continuous line is the prediction for GRBs of known z , selected with the same criteria.

- The time–energy correlation of the pulses: the pulse duration decreases like $\sim E^{-0.4}$ and peaks earlier the higher the energy interval.
- Various correlations between pairs of the following observables: photon fluence, energy fluence, peak intensity and luminosity, photon energy at peak intensity or luminosity, and pulse duration.
- The possibly large polarization of the γ rays.

Two examples of these predictions⁵ are given in Fig. (6): on the left, the spectrum of the γ -rays of a GRB, exponentially evolving from $dN/dE \sim E^{-1}$ to $\sim E^{-2.1}$ at a “peak energy” whose observed and predicted distributions are shown on the right.

XRFs are simply GRBs viewed at larger angles, which makes their fluence and the energy of their quanta smaller, and their time structure less rugged⁶.

3.3. Afterglows and Cosmic Rays

While a CB crosses the domain permeated by the ambient light surrounding its parent SN, it is assumed to be expanding at a speed comparable to that of sound in a relativistic plasma ($c/\sqrt{3}$). Its typical baryon number is that of half of Mercury $N_{CB} \sim 10^{50}$, its start-up LF is $\gamma_0 \sim 10^3$ (both ascertained from the properties of AGs, and of the GRB’s γ rays). In their voyage, CBs continuously intercept the electrons and nuclei of the interstellar medium (ISM), previously ionized by the GRB’s γ rays. In seconds of (highly Doppler-foreshortened) observer’s time, such an expanding CB becomes “collisionless”, that is, its radius becomes bigger than a typical nucleus-nucleus interaction length. But it still interacts with the charged

ISM particles it encounters, for it contains a strong magnetic field^b.

If the nuclei entering a CB are magnetically “scrambled” and are reemitted isotropically in the CB’s rest system, a radial loss of momentum results. The rate of such a loss corresponds to an inwards radial force on the CB. In our analysis of GRB AGs, we made two assumptions: that this force counteracts the initial expansion, and that when the radius stabilizes, the inwards pressure is in equilibrium with the pressure of the CB’s magnetic field plus that of the fagocitated ISM nuclei that generate it. This results in values for the asymptotic CB radius ($R_{CB} \sim 10^{14}$ cm for typical parameters) and its time-dependent magnetic-field strength⁸:

$$B_{CB}[\gamma(t)] = 3 \text{ Gauss} \frac{\gamma(t)}{10^3} \left(\frac{n_p}{10^{-3} \text{ cm}^{-3}} \right)^{1/2}, \quad (1)$$

where n_p is the ISM number density, normalized to a value characteristic of the “superbubble” domains in which SNe and GRBs are born. Our two assumptions are no doubt extreme oversimplifications, but they are to be judged in light of two facts: 1) The extremely simple ensuing analysis of the elaborate time and frequency dependence of AGs, which are dominated by synchrotron radiation of electrons in the field of Eq. (1); 2) There must be a reason why the CBs emitted by certain objects appear not to expand significantly, as in the example Fig. (1).

As a CB pierces through the ISM, its LF, $\gamma(t)$, continuously diminishes, as its energy is dominantly transferred to scattered ISM nuclei, and subdominantly to scattered electrons and synchrotron photons. All these reemitted particles, in the rest system of the host galaxy, are forward-peaked in a distribution of characteristic opening angle $1/\gamma(t)$. In the lower Fig. (1) the two jets of Pictor A are shown, with contour plots corresponding to radio-intensity levels³⁴. We interpret this radio emission as the synchrotron radiation of the CB-generated *Cosmic-Ray electrons* in the ambient magnetic fields. Similarly, the CBs of Pictor A must be scattering the ambient nuclei, and converting them into *Cosmic-Ray Nuclei*.

The range of a CB is governed by the rate at which it loses momentum by encountering ISM particles and catapulting them into CRs. The initial LF, $\gamma_0 \sim 10^3$, is typically halved in a fraction of a kpc, while a CB becomes non-relativistic only at distances of 10’s or even 100’s of kpc, well into a galaxy’s halo or beyond. The CRs of the CB model are deposited along the long *line* of flight of CBs, in contradistinction with those of the standard models, in which the CRs are generated by SN shocks³⁵, at the “*points*” where they occur in “active” regions of stellar birth and death. In the CB model no reacceleration mechanisms far from the CR birth-sites need be invoked to accomodate the data. This is most relevant for electrons, which lose energy fast (and locally) by ICS and synchrotron radiation⁹.

^bNumerical analysis of the merging of two plasmas at a high relative γ , based on following each particle’s individual trajectories as governed by the Lorentz force and Maxwell’s equations, demonstrate the generation of such turbulent magnetic fields, as well as the “Fermi” acceleration of particles, in the total *absence* of shocks³³, to a power law spectrum: $dN/dE \approx E^{-\beta_s}$, with $\beta_s \sim 2.2$.

3.4. Apparent “hyperluminal” motions

An object moving at a speed $v = \beta c$, at an angle θ relative to a very distant observer, appears to move³⁶ transversally to the line of sight at a velocity $v_{\perp} = c \beta \sin \theta / (1 - \beta \cos \theta)$, which can be greater than c . The “approaching” CBs of quasars and μ -quasars are often “superluminal”. The CBs of GRBs⁴, for which $v_{\perp}/c \sim \mathcal{O}(10^3)$ at early times, should be *hyperluminal*.

Only long-baseline radio-interferometry has sufficient angular resolution to detect the motion of the CBs of cosmological GRBs or XRFs. The hope is to observe the motion of a CB relative to the “fixed” sky, or the *relative* motion of two CBs, moving in roughly the same direction, with large but unequal LFs.

Such measurements have been attempted in the case of GRB 030329, which had two observed CBs in the GRB (two γ pulses) and in its AG, see Fig. (4). In all observations at various times and frequencies—but one—only one source was observed, whose motion in the sky, according to the observers “is incompatible with the CB model”³⁷. If the single source is the slower of the two CBs, this conclusion is invalid⁴¹, as shown in Fig. (7a). At day ~ 51 two sources were seen at a single frequency³⁷. At that same date, the radio³⁸ and optical³⁹ AGs underwent rebrightenings, extraordinarily large in the optical case. We interpret such rebrightenings as the effect of a CB crossing an ISM density inhomogeneity⁷. If the CB that rebrightens at day 51 is the “second component”, the *prediction*^{40,41} for the angular separation between the two CBs agrees with the observation, see Fig. (7b).

The authors of the above observations conclude³⁷ that “*This [second] component requires a high average velocity of $19c$ and cannot be readily explained by any of the standard models. Since it is only seen at a single frequency, it is **remotely possible** that this image is an artifact of the calibration.*” Our referees conclude that these observations of hyperluminal relative motions are **surely** artefacts and do not deserve an explanation. Only future observations may decide. They might be simpler to make for XRFs than for GRBs, since the observer’s angles and subsequent hyperluminal velocities of the former are the larger⁶.

4. The Gamma “Background” Radiation, and the CR electrons

The existence of an isotropic, diffuse gamma background radiation (GBR, confusingly similar to GRB) was first suggested by data from the SAS 2 satellite⁴². The EGRET/CRGO instrument confirmed it: “*by removal of point sources and of the galactic-disk and galactic-centre emission, and after an extrapolation to zero local column density*”, a uniformly distributed GBR was found, of alleged extragalactic origin⁴³. Above an energy of ~ 10 MeV, this radiation has a featureless spectrum, shown in Fig. (8), which is very well described by a simple power-law form, $dF/dE \propto E^{-\beta_{\text{GBR}}}$, with $\beta_{\text{GBR}} \approx 2.10 \pm 0.03$.

There is no consensus on what the origin of the GBR is. The proposed candidate sources range from the rather conventional (e.g. active galaxies⁴⁴) to the decisively speculative (e.g. primordial black hole evaporation⁴⁵). A “cosmological” origin is

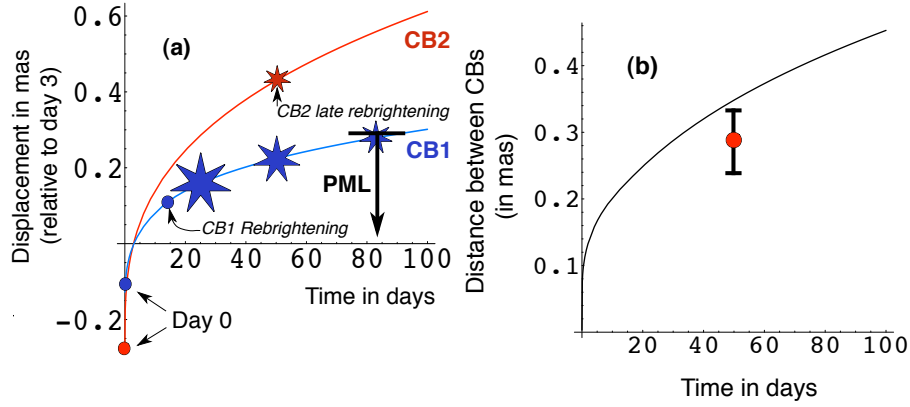


Fig. 7. (a) The predicted angular displacement in the sky (in mas) of the two CBs of GRB 030329, as a function of observer’s time from the first day of VLBI radio observations, day ~ 3 . The positions at day 0, the start-up time of the successive predicted rebrightenings of the slower CB1, the observed time of the intense late rebrightening of the faster CB2, as well as the observed fluences at 15.3 GHz of the two sources resolved on day 51 —70% and 30% of the total— are illustrated [the CBs are labeled as in Fig. (4)]. The proper motion limit (PML) of the “main component” is also shown. (b) The predicted angular distance between the two CBs as a function of time, and its measurement at day 51.

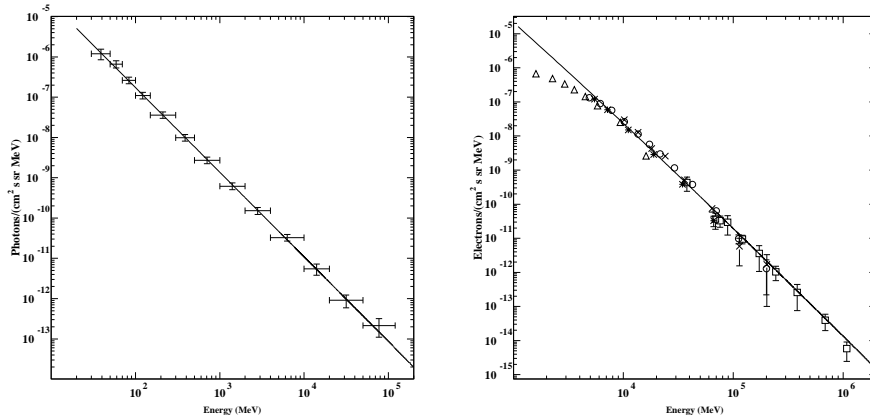


Fig. 8. Left: Comparison between the spectrum of the GBR, measured by EGRET, and the prediction (the line) for ICS of starlight and the CMB by CR electrons. Right: The primary CR electron spectrum. The slope is the prediction, the magnitude is normalized to the data.

the oldest and most noble putative ancestry, but though the GBR index β_{GBR} is uncannily direction-independent, the EGRET GBR flux in directions above the galactic disk and centre shows significant anisotropies, correlated with our position relative to the centre of the Galaxy⁴⁶. How does the GBR relate to CRs?

Below a few GeV, the local spectrum of CRs is affected by the solar wind and the Earth's magnetic field, its modelling is elaborate. Above ~ 5 GeV, the spectrum of CR electrons, shown in Fig. (8), is well fit by a power law⁴⁷: $dF/dE \propto E^{-\beta_e}$, with $\beta_e \approx 3.2 \pm 0.1$. The nuclear CR spectrum, above ~ 10 GeV and up to the “knee” at $\sim 3 \times 10^6$ GeV, is also a single power law: $dF/dE \propto E^{-\beta_p}$, with $\beta_p \approx 2.70 \pm 0.05$ ($\sim 96\%$ of these nuclei are protons, at a fixed energy *per nucleon*).

As discussed in detail in Section 7.1, CBs accelerate the ISM electrons and nuclei they encounter in their path as a “magnetic-racket” would, imparting to all species the same distribution of LFs γ . This means that the **source** spectra of (relativistic) nuclei and electrons have the same energy dependence: $dF/dE \propto E^{-\beta_s}$, with a species-independent β_s . The observed spectra are not the source spectra. The nuclear flux is modulated by the energy dependence of the CR confinement-time, τ_{conf} , in the magnetized disk and halo of the galaxy, affecting the different species in the same way, *at fixed E/Z* , with Z the nuclear charge. Confinement effects are not well understood, but observations of astrophysical and solar plasmas and of CR abundances as functions of energy indicate that⁴⁸:

$$\tau_{\text{conf}} \propto (Z/E)^c, \quad (2)$$

with $c \sim 0.5 \pm 0.1$ at the low energies at which the CR composition is well measured. This means that $\beta_s = \beta_p - c \sim 2.2$, as in the results quoted in footnote *b*.

Above a few GeV, the electron spectrum is dominantly modulated by ICS on starlight and on the microwave background radiation, the corresponding electron “cooling” time being shorter than their confinement time. For an equilibrium situation between electron CR generation and ICS cooling, this implies that $\beta_e = \beta_s + 1 \sim 3.2$, a prediction⁹ in perfect agreement with observation, as in Fig. (8). In the CB model, the Compton upscattered photons **are** the GBR, and their spectrum is a power law with a predicted⁹ index $\beta_{\text{GBR}} = (\beta_e + 1)/2 \sim 2.1$, also in agreement with the data, as in Fig. (8). Cannonballss deposit CRs along their linear trajectories, which extend well beyond the Galaxy's disk onto the halo and beyond. The observed non-uniform (i.e. non-cosmological) distribution of GRB flux in intensity, latitude and longitude is well reproduced⁹ for an ellipsoidal CR halo of characteristic height ~ 20 kpc, and radius ~ 35 kpc, see Fig. (9).

5. The CR Luminosity of the Galaxy

If the CRs are chiefly Galactic in origin, their accelerators must compensate for the escape of CRs from the Galaxy, in order to sustain the observed CR intensity: it is known from meteorite records that the CR flux has been fairly steady for the past few giga-years⁴⁹. The Milky Way's luminosity in CRs must therefore satisfy:

$$L_{\text{CR}} \approx L_p = \frac{4\pi}{c} \int \frac{1}{\tau_{\text{conf}}} E \frac{dF_p}{dE} dE dV \sim \frac{4\pi}{c} \int \bar{\rho} dV \int \frac{1}{X} E \frac{dF_p}{dE} dE, \quad (3)$$

where the last result is the standard estimate, thus obtained: The mean column density X traversed by CRs before they reach the Earth can be extracted⁴⁸ from the

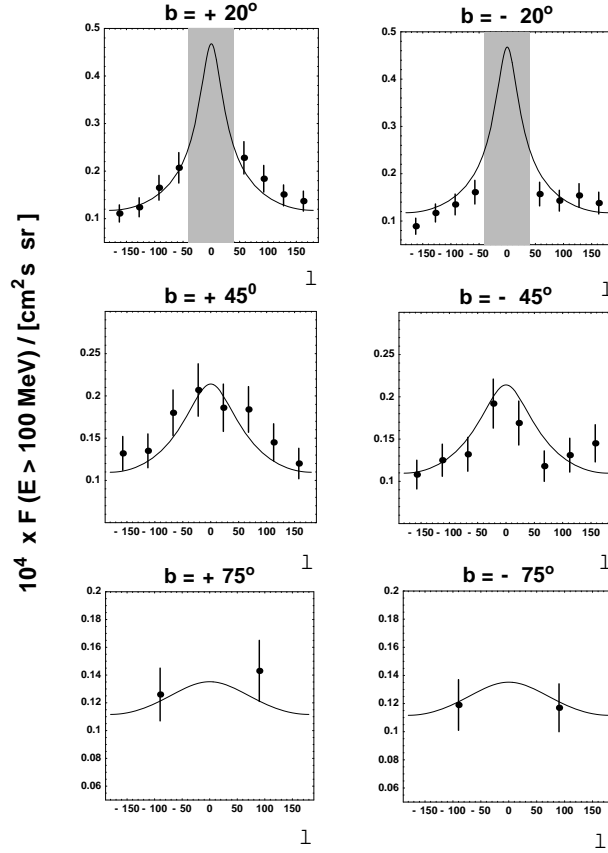


Fig. 9. The flux of GBR photons above 100 MeV: comparison between EGRET data and our model, as functions of latitude at various fixed longitudes. The grey domain is EGRET's “mask”.

observed ratios of primary CRs to secondaries (products of spallation). With use of $X = \int \rho dx \sim \bar{\rho} c \tau_{\text{conf}}$ one can extract the product of $\tau_{\text{conf}}(E)$ and a path-averaged density $\bar{\rho}$. If the local values of X and dF_p/dE are representative of the Galactic values dominating the first integral in Eq. (3), the final result follows. Assume the path-averaged $\bar{\rho}$ to be close to the average density ρ of neutral and ionized gas in the Galaxy, so that $\int \bar{\rho} dV$ is the total mass of Galactic gas, estimated⁴⁹ to be $5 \times 10^9 M_\odot$. The numerical result is⁵⁰:

$$L_{CR} \sim 1.5 \times 10^{41} \text{ erg s}^{-1}. \quad (4)$$

In the CB model L_{CR} can be estimated from the electron CR density involved in its successful description of the GBR, assuming the local observed ratio of proton to electron fluxes to be representative of the Galactic average. It can also be estimated from the rate of Galactic SNe and the typical energy in their jets of CBs. The results of these two estimates agree⁵¹, but they are over one order of magnitude larger than Eq. (4). This is not a contradiction, for the CB-model effective volume

in Eq. (3) is much bigger than in the standard picture, wherein CRs are confined to the Galactic disk. The CB-model value of τ_{conf} implied by these considerations is also one order of magnitude larger than the standard result, based on the ratios of stable to unstable isotopes⁵¹. This alterity can be understood⁵² in the same terms: the stable CRs may spend much of their travel time in the Galaxy’s halo, which in the CB-model is magnetized by the very flux of CRs that the CBs deposit in it.

6. Cooling Flows, or “Warming Rays”?

The radiative cooling time of the X-ray-emitting plasma near the center of many clusters of galaxies is shorter than the age of the cluster, but neither the expected large drop in central temperature –nor the expected mass flow towards the pressure-depleted cluster centers– are observed⁵³. In the CB model, the energy is supplied to the plasma by the CRs produced by the cluster’s galaxies. This solution requires an energy deposition more intense and more distributed than in conventional CR models, but this is precisely, as we have just discussed, what the model offers. The X-ray energy emitted by clusters is supplied, in a quasi-steady state, by the CRs, which act as “warming rays”¹¹.

The temperature distribution in the intracluster space is successfully predicted from the measured plasma-density distribution, as in the example⁵⁴ of Fig. (10). Four other puzzling features of clusters can also be explained in simple terms: the discrepancy between their “virial” and “lensing” masses, their large magnetic fields, the correlation between their optical and X-ray luminosities, and the non-thermal tail of their X-ray spectrum¹¹.

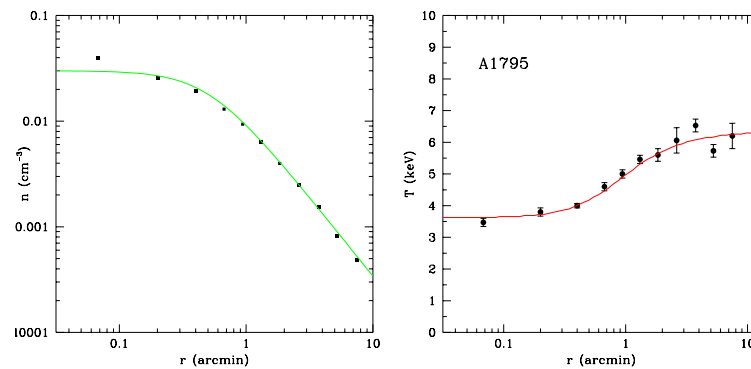


Fig. 10. Observed and fit density profile of the cluster A1795, and its observed and CB-model-predicted temperature distribution.

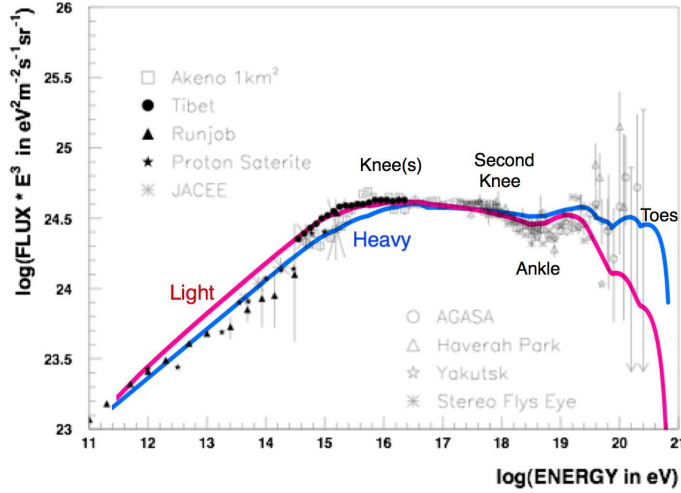


Fig. 11. The “all-particle” CR spectrum. The “light” and “heavy” lines are predictions for the two CR abundances discussed in Section 7.9. Only one parameter was adjusted, see Section 7.5.

7. Back to Cosmic Rays

It is customary to “renormalize” somewhat the energy calibration of different experiments to make their flux measurements look in better agreement; and to present the data as the flux times a power of energy, to emphasize the “features” of the spectrum and the corresponding changes in the power “index”. This is done in Fig. (11) for the “all-particle” spectrum⁵⁵, showing the “knee” at $(2 \text{ to } 3) \times 10^{15}$ eV, the “second knee” at $\sim 5 \times 10^{17}$ eV and the “ankle” at $\sim 3 \times 10^{18}$ eV. The purpose of this section is to outline how these features, and the changes of CR composition with energy, are simple consequences of the CB model of CR production.

7.1. “Collisionless magnetic rackets”

In an elastic collision of a relativistic CB of LF γ with (much lighter) ISM electrons or ions at rest, the light recoiling particles (of mass M) have an energy spectrum extending up to $E = 2\gamma^2 M c^2$. This is a *magnetic-racket accelerator* of gorgeous efficiency: the ISM particles reach up to $\Gamma = 2\gamma^2$. Single elastic scattering of target particles at rest is not the whole story, for CBs may collide with previously-accelerated CRs. Also, as in footnote *b*, CBs may internally “Fermi”-accelerate particles, before reemitting them. The extreme in which the first process is dominant has been studied by Dar¹². Here, the opposite extreme is discussed for the first time. A bit coincidentally, the two extremes lead to very similar results.

In our study of GRB AGs, we assumed that the AG is dominated by electron synchrotron radiation in the magnetic field of Eq. (1). We also used the simplifying

assumption that half of the electrons within a CB are unaccelerated, while the other half are accelerated, in the CB's rest system, to a source spectrum $dN/d\gamma_e \propto \gamma_e^{-\beta_s} \Theta(\gamma_e - \gamma)$, with $\beta_s = 2.2$ (as in footnote *b*), and $\gamma = \gamma(t)$ the LF or the incoming electrons: the one of the CB in the SN rest system. These assumptions led to the prediction of a wide-band AG spectrum in excellent agreement with observations⁸. Here, I make similar assumptions: the LF distributions of the ISM nuclei intercepted, magnetically deflected, partially accelerated and reemitted by a CB are *identical* to those of electrons (but for the effect of electron cooling by synchrotron radiation). The only other difference is that we shall be concerned with nuclei of up to very high energies, for which the “Larmor” limit —on the maximum possible acceleration within a CB— will play a role.

7.2. Elastic scattering and the “A-flavoured knees”

Let m be the mass of the proton and $m A$ the approximate mass of a nucleus of atomic weight A , which, abusing of the quark analogy, I shall refer to as “flavour”. The ISM nuclei recoiling from an elastic scattering with a CB of Lorentz factor γ have energies in the range $m A \leq E_A \leq 2 m A \gamma^2$. Since the initial Lorentz factors of CBs, as extracted from the analysis of their AGs^{7,8} and/or “peak energies”^{4,5} peak at $\gamma_0 \sim 10^3$ and have a narrow distribution extending up to $\gamma_0 \sim 1.5 \times 10^3$, the spectrum of nuclei elastically scattered by CBs should end at a maximum energy

$$E[\text{knee}] \sim (2 \text{ to } 4) 10^6 A \text{ GeV}. \quad (5)$$

We shall see anon that $E[\text{knee}]$ is also the position at which the spectrum of inelastically scattered nuclei changes its slope.

The individual spectra of abundant elements and groups of CRs are shown in Fig. (12). Preliminary CR composition data from the KASCADE experiment⁵⁶ indicate that there is indeed a change of slope of the individual particle spectra at the values predicted in Eq. (5), but the data are not yet good enough to establish the predicted linear A -dependence, or to distinguish it from a putative Z -dependence.

7.3. “Accelerated scattering” and the “Z-flavoured toe-nails”

The spectrum of Fermi-accelerated particles within a CB cannot extend beyond the Z -dependent energy at which their Larmor radius in the CB-field of Eq. (1) is larger than the CB's radius. For typical parameters:

$$E[\text{Larmor}] \simeq 9 \times 10^{16} Z \text{ eV} \frac{B_{CB}[\gamma_0]}{3 \text{ G}} \frac{R_{CB}}{10^{14} \text{ cm}}. \quad (6)$$

The ISM nuclei exiting a CB after having being accelerated within have energies extending up to $E[\text{toe}] = 2 \gamma_0 E[\text{Larmor}]$, that is:

$$E[\text{toe}] \sim (2 \text{ to } 6) 10^{11} Z \text{ GeV}, \quad (7)$$

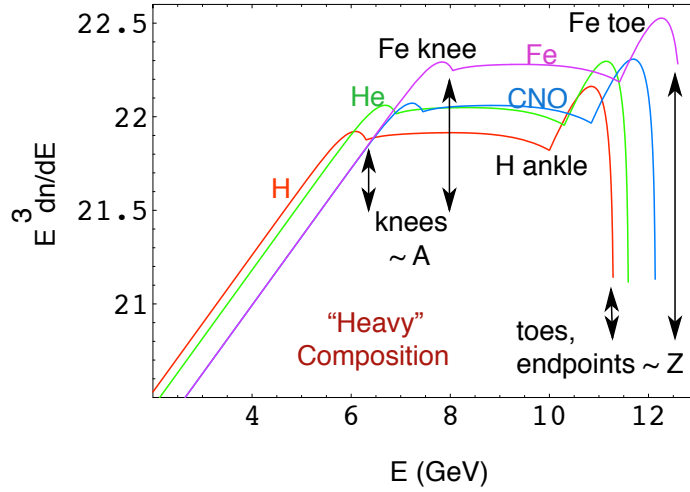


Fig. 12. Log-log plot of the predicted $E^3 dN/dE$ spectra of H, He, the CNO group and the Fe group, for the “heavy” CR relative abundances of Section 7.9. The relative abundances become more “metallic” at the knees and again above the ankle. Only one parameter was adjusted.

which is the maximum energy to which the CB mechanism we have discussed is capable of accelerating CRs. Notice that the predicted “toes” at the spectral end scale as Z , not like A , as the “knees” do, as illustrated in Fig. (12).

The energy $E[\text{toe}]$ for Fe nuclei is comparable to the maximum observed energies in the CR spectrum. There is some evidence⁵⁷ for changes of composition above the ankle, compatible with those implied by Fig. (12). But the extraction of relative CR abundances at very high energies is a difficult task.

7.4. The deceleration of CBs in the ISM

Consider a CB of initial mass M_0 , traveling through the ISM at an instantaneous LF γ . Let a be the ratio between the average energy of a nucleus exiting a CB in rest system and the energy at which the nucleus entered, so that $\langle \gamma_{out} \rangle \equiv a\gamma$. For elastic scattering, $a = 1$; for nuclei fagocitated by the CB, $a = 0$; and for those Fermi-accelerated within the CB, $a > 1$. Let \bar{a} be the mean value in the average over these processes, and \bar{A} the mean weight in the ISM density distribution dn_A . For $\gamma^2 \gg 1$, energy-momentum conservation implies a CB’s deceleration law:

$$\frac{d\gamma}{\gamma^k} \simeq -\frac{m}{M_0} \gamma_0^{\bar{a}-1} \bar{A} dn_A, \quad (8)$$

$$k \equiv 3 - \bar{a}. \quad (9)$$

To compute the spectrum of the CRs produced by a CB in its voyage through the ISM we have to let the CB decelerate from $\gamma = \gamma_0$ to $\gamma \sim 1$, tantamount to integrating the CR spectra at local values of γ with a weight factor $dn_A \propto d\gamma/\gamma^k$.

The value of k in Eq. (9) cannot be ascertained with confidence. One reason is the averaging over the quoted processes. Three other reasons are: 1) The nucleus-CB elastic scatterings may not be isotropic. If the cross-section is modeled as a power-law in momentum transfer, $d\sigma \propto (1 + \beta \cos \alpha)^{-a_1}$, one obtains an approximate “effective” deceleration law $d\gamma/\gamma^{k_1}$, with $k_1 > k$. 2) The reemission of accelerated nuclei may be delayed, so that they exit the CB at $\gamma_{exit} < \gamma$. If the γ_{exit} distribution is modeled as a power law $\gamma_{exit}^{-a_2}$, one obtains again an approximate “effective” deceleration law $d\gamma/\gamma^{k_2}$, with $k_2 > k$. 3) Slow CBs would be unobservable in GRBs or their AGs, for the fluences are biased towards large γ . Microquasars may also contribute low- γ_0 CR-generating CBs. If the γ_0 distribution is modeled as a power law, once again the “effective” value of k is increased. All in all, we may expect $k \sim 3$, but we cannot predetermine its value.

7.5. The spectrum of elastically-scattered CRs

Let the elastically scattered CRs, exiting a CB in its rest system with the decelerating instantaneous value of γ , be isotropically emitted, with a constant $d\sigma/d\cos\alpha$: we have seen that a reasonable non-isotropy only leads to an increase of k . Boosted by the CB’s motion, the instantaneous CR spectrum in the SN rest system is:

$$\frac{dN}{d\gamma_A} \propto \int_{-1}^1 \frac{d\cos\alpha}{2} \delta[\gamma_A - \gamma \gamma (1 + \cos\alpha)] = \frac{1}{2\gamma^2} \Theta[2\gamma^2 - \gamma_A]. \quad (10)$$

To obtain the total “elastic” CR spectrum, integrate over the CB’s trajectory:

$$\int_{\text{traj}} dn_A \frac{dN}{d\gamma_A} \propto \int_1^{\gamma_0} \frac{d\gamma}{\gamma^k} \frac{dN}{d\gamma_A} \propto \left(\frac{1}{\gamma_A}\right)^{\frac{k+1}{2}} \left[1 - \left(\frac{\gamma_A}{2\gamma_0^2}\right)^{\frac{k+1}{2}}\right] \Theta[2\gamma_0^2 - \gamma_A]. \quad (11)$$

This elastic-scattering contribution extends up to $\gamma_A = 2\gamma_0^2$, as announced in Section 7.2. For energies below these knees, the Galaxy confines CRs so that the result of Eq. (11) is to be modified by the multiplicative factor $\propto 1/\gamma_A^c$ of Eq. (2). The observed slope $\beta \sim 2.7$ of the CR spectra below the knees is reproduced for $c + (k+1)/2 = \beta$. In practice, this combination of parameters is the *only quantity* chosen by hand in predicting the all-particle and individual CR spectra.

7.6. The spectrum of CB-accelerated CRs

The spectrum of nuclei accelerated within a CB is “flavour-blind” in the variable γ_A , and of the form $dN/d\gamma_A \propto \gamma_A^{-\beta_s} \Theta(\gamma_A - \gamma) \Theta(b\gamma - \gamma_A)$, with $\beta_s = 2.2$, and $\gamma = \gamma(t)$. The second Θ function is the Larmor cutoff, for typical parameters $b \sim 10^5$. Boosted to the SN rest system, the instantaneous CR spectrum is:

$$\int_{\gamma}^{b\gamma} \frac{d\bar{\gamma}}{\bar{\gamma}^{\beta_s}} \int_{-1}^1 \frac{d\cos\alpha}{2} \delta[\gamma_A - \bar{\gamma} \gamma (1 + \cos\alpha)] = \int_{\text{Max}[\gamma, \sqrt{\gamma_A/(2\gamma)}]}^{b\gamma} \frac{d\bar{\gamma}}{\bar{\gamma}^{\beta_s}} \frac{1}{2\gamma\bar{\gamma}}. \quad (12)$$

This spectrum must still be integrated over the CB’s trajectory, as in Eq. (11), and corrected for confinement in the Galaxy. The result is again simple and analytical,

but a bit long to report here. Below the knee, it has the same power-law behaviour as the elastic contribution. The effect of the discontinuity in the lower limit of integration in Eq. (12) survives in the trajectory-integrated result as a predicted smooth change in slope by $\Delta\beta \sim 0.3$ at $\gamma_A = 2\gamma_0^2$, which is what is observed, see Figs. (11,12). The spectra extend all the way to the Larmor cutoff(s) of Eq. (6).

7.7. *Galactic confinement: the ankle(s)*

The interpretation of the ankle(s) in the CB model is conventional: they are the Z -dependent energies at which the Galaxy and its magnetized halo no longer confine cosmic rays². For $B \sim 3 \mu\text{G}$, the position of the ankle(s) is at:

$$E[\text{ankle}] \sim 3 \times 10^9 Z \text{ GeV}. \quad (13)$$

Cannonballs deposit CRs along their trajectories, which extend to the halo and beyond. Galactic CRs above $E = E[\text{ankle}]$ escape. Instead of a cutoff, a change to a harder spectrum is seen, which must therefore be an *extragalactic flux*. I have assumed in Figs. (11,12) that the spectrum of CRs above the ankles is the source spectrum, corresponding to a sharp transition from $c \sim 0.5$ to $c = 0$ in Eq. (2).

7.8. *GZK modulations*

Cosmic rays having travelled in intergalactic space along straight or curved trajectories for sufficiently long times should be subject to rather sharp energy-cutoffs, the well known GZK effect⁵⁸. Such cutoffs would act as extra “chinese lady shoes” further constraining the “toe-nail” cutoffs we have discussed. Are these GZK cutoffs expected in the CB model? It depends on Galactic “accessibility”.

It is difficult to ascertain the probability that extragalactic CRs of energies *below* the ankle penetrate the Galaxy, if only because in the CB-model there is an exuding Galactic “wind” of CRs and their accompanying magnetic fields. If the Galaxy is quite “accessible”, a good fraction of the observed lower-energy CRs would be extragalactic (not a dominant fraction, for otherwise redshift effects would erase the sharp features of the spectrum). A large extragalactic contribution implies long “look-back” times and, consequently, potentially observable GZK modulations. A small contribution implies short look-back times, no GZK effects, but the possibility of observing relatively well-located point sources in the Virgo-cluster “neighbourhood”. Thus, in a sense, this is a “no-lose” situation: some new effect ought to be found at the highest observable energies.

7.9. *CR abundances*

Let n_A be the number density of the “target” ISM nuclei converted by the CBs’ passage into CRs. The source spectra $dn_A/d\gamma$, are flavour-blind, so that the CR confinement-modified energy spectra are of the form:

$$\frac{dN_A}{dE} \propto \frac{1}{Am} \frac{dn_A}{d\gamma} \left(\frac{Z}{E} \right)^c \propto K n_A A^{\beta-c-1} Z^c E^{-\beta}, \quad (14)$$

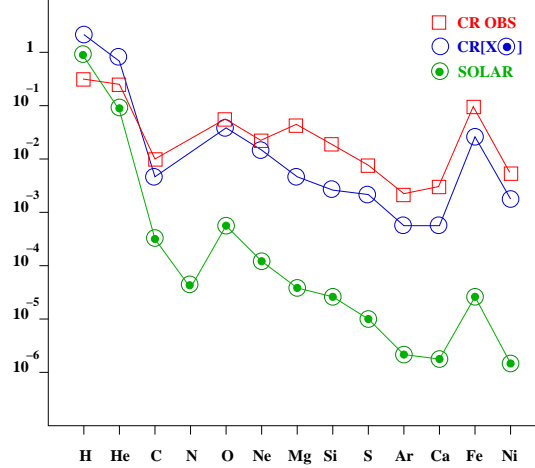


Fig. 13. The relative abundances of primary CRs, from H to Ni. The (green) dotted circles are solar-neighbourhood ISM abundances. The (blue) circles are the predictions, with input solar abundances. The (red) squares are observed CR abundances below ~ 1 TeV.

with K a universal, composition-independent constant. Below the knee(s) $\beta = 2.7$ and $c \sim 0.5$ (I have ignored a weak composition-dependence of β , discussed by Dar¹²). In Fig. (13) the observed abundances of the most relevant *primary* CRs, up to Ni, are compared with the *solar* abundances, which are used as input to Eq. (14), whose results are also shown. In Figs. (11) and (12) I have referred to the predicted and observed compositions of Fig. (13) as “light” and “heavy”. The predictions are seen to fail at the large-metallicity end by a factor of ~ 3 . This is what is expected, for CBs travel much of the time in a star-burst region and a local superbubble that are known (within very large errors) to have thrice the metallicity of the solar neighbourhood. Given this uncertainty, it may be premature to do a complete calculation taking into account CR propagation and the production of CRs with a broad spectral distribution at the different points of many CB trajectories crossing a variety of ISM domains. After all, our aim is to understand all of the salient features of the CR conundrum, not its nitty-gritty details!

8. Conclusions and further predictions

We have argued that a large variety of high-energy astrophysical phenomena are interrelated, and easy to understand in extremely simple terms. The unifying concept is the ejection of relativistic blobs of matter in violent processes of accretion onto compact objects. The inspiring observations are those of quasars and microquasars. We have assumed that SNe axially eject very relativistic CBs of ordinary plasma, as their finite supply of matter catastrophically accreting onto their central compact object is used up. This assumption, complemented by a variety of observations of

pre-SN environments, explains not only the SN/GRB association, but the properties of GRBs and XRFs. The underlying process is ubiquitous in astrophysics: (inverse) Compton scattering. None of the parameters involved in these predictions are put in by hand: they either rely on observations (e.g. the early luminosity of a SN), or are borrowed from the CB-model analysis of GRB afterglows (the distribution of CB Lorentz factors and of the CB-motion angles relative to the line of sight to observers on our planet, and the typical mass of a CB).

The analysis of GRB AGs requires extra assumptions that are no doubt oversimplifications: the way a relativistically expanding blob of plasma reaches an equilibrium radius as the process of radial reemission of the “collisionlessly” scattered charged ISM particles quenches the expansion, and the way in which the CB’s magnetic-field pressure thereafter compensates the inwards force of the radially expanding particles. But the ensuing description of AGs as the synchrotron radiation from the ISM electrons entering the CBs is simple and successful: the AG light curves and wide-band spectra of all GRBs of known redshift are well fit and, when predicted, correct.

Several predictions of the CB model of GRBs, we contend, are supported by the data, but require further corroboration. One is the hyperluminal motion of the CBs themselves, which may be easier to detect in XRFs: when not too far, they are simply GRBs seen at larger angles. Another prediction concerns the AG X-ray lines, which in the CB model are not the generally-assumed lines of Fe and other intermediate elements, but the highly Doppler-boosted lines of light elements, notably H Ly- α lines⁵⁹. Since CBs decelerate in the ISM as they emit these radiations, the lines should evolve towards lower frequencies in a predicted fashion⁵⁹.

On the basis of much less observational input, we propose⁵ that short-duration GRBs are associated with Type Ia SNe (30% of the SNe are of this type, 30% of GRBs are short). If the observers did not give up so early in attempting to discover the weak AG of short GRBs –but waited for a few weeks for the peak SN light– the SN ought to be observable. That would be good news for cosmology, even if GRB-associated Type Ia SNe deviate from the usual “standard candle” properties: in the CB model SNe are roughly axially –but not spherically– symmetric. SN1998bw and the other almost identical SNe associated with GRBs (some spectroscopically established), are ordinary SNe seen very close to their axis. Both Type Ia and core-collapse SNe ought to be closer to standard “torch-lights” than to “candles”.

We have also seen that the CB-model explains the shape of the CR electron spectrum, and the related spectrum and angular distribution of the GBR, most of which is not “cosmological”: it is associated at high latitudes with our own Galactic halo. Higher-energy data on CR electrons and the GBR might confirm the model by discovering the predicted “knees” in the corresponding spectra⁹. Seeing the “GBR” light from the halo of Andromeda would also be quite a coup⁹.

We do not have further predictions on the properties of X-ray emitting rich clusters, except that Cooling Flows are not cooling flows. It is the mechanism of

heating that we have identified: CB-induced CRs. The rest of the properties of these clusters are also well and simply explained¹¹. There should be no substantial flow of plasma, no substantial shock-induced heating...

The CB model of CRs is rather successful, considering that only one parameter was adjusted. Clearly the results could be improved, as better data are gathered (e.g. on composition at all energies above ~ 1 TeV). Many simplifying choices were made: a spacially constant ISM composition, a 50-50 contribution of nuclei accelerated and unaccelerated within a CB, a naïve energy dependence of the Galactic-confinement factor... Even so, the distribution of CRs in the Galaxy, their total luminosity, the broken power-law spectra with their observed slopes, the position of the knee(s) and ankle(s), and the alleged variations of composition with energy are all explained in terms of simple physics. Naturally, “life” may be more complicated, e.g. nearby SNe could contribute low-energy CRs, accelerated by conventional shock mechanisms³⁵. There is no tell-tale CB-model-specific prediction concerning CRs, except that they are deposited along very long lines exiting star-death regions, as opposed to points in these very regions, as in standard models. This prediction might be testable in the search for line inhomogeneities in the radiation from CR electrons.

The CB model is not a *theory* of practically all high-energy astrophysical phenomena. It is lacking a deeper theoretical understanding of the magneto-dynamics within a CB; and of *cannons* themselves: the engines generating the mighty ejections of compact astrophysical objects.

Acknowledgements

I thank Shlomo Dado and Arnon Dar for a long and fruitful collaboration, and Nick Antoniou, Andy Cohen, Sergio Colafrancesco, Shelly Glashow and Reiner Plaga for collaboration and/or patient discussions.

References

1. A. Dar, B. Z. Kozlowsky, S. Nussinov and R. Ramaty, *ApJ* **388**, 164 (1992).
2. A. Dar and R. Plaga, *A&A* **349**, 259 (1999).
3. N. J. Shaviv and A. Dar, *ApJ* **447**, 863 (1995).
4. A. Dar and A. De Rújula, astro-ph/0008474
5. A. Dar and A. De Rújula, astro-ph/0308248, to be published in *Phys. Reps.*
6. S. Dado, A. Dar and A. De Rújula, *A&A* **422**, 381 (2004).
7. S. Dado, A. Dar and A. De Rújula, *A&A* **388**, 1079 (2002).
8. S. Dado, A. Dar and A. De Rújula, *A&A* **401**, 243 (2003).
9. A. Dar and A. De Rújula, *MNRAS* **323**, 391 (2001).
10. A. Dar and A. De Rújula, *ApJ* **547**, L33 (2001).
11. S. Colafrancesco, A. Dar and A. De Rújula, *A&A* **413**, 441 (2004).
12. A. Dar, astro-ph/0408310
13. A. S. Wilson, A. J. Young and P. L. Shopbell, *ApJ* **547**, 740 (2001).
14. I. F. Mirabel and L. F. Rodríguez, *Ann. Rev. Astron. & Astroph.* **37**, 409 (1999).
15. T. Kotani et al., *Pub. Astronom. Soc. Japan* **48**, 619 (1996).
16. A. De Rújula, *Phys. Lett.* **193**, 514 (1987).

22 *A. De Rújula*

17. P. Nisenson and C. Papaliolios, *ApJ* **518**, L29 (1999).
18. T.J. Galama, et al. *Nature* **395**, 670 (1998).
19. M. Schmidt, *ApJ* **559**, L79 (2001).
20. E. Capellaro, *Supernovae and GRBs* (ed. K. W. Weiler, Springer Berlin) p. 37 (2003).
21. P. Soffitta, et al. *IAU Circ.* 6884 (1998).
22. K. Iwamoto, et al. *Nature* **395**, 672 (1998).
23. S. Dado and A. Dar, astro-ph/0409466.
24. S. Dado, A. Dar and A. De Rújula, *ApJ* **572**, L143 (2002).
S. Dado, A. Dar and A. De Rújula, *A&A* **393**, L25 (2002).
25. S. Dado, A. Dar and A. De Rújula, *ApJ* **593**, 961 (2003).
S. Dado, A. Dar and A. De Rújula, *ApJL* **594**, L89 (2003).
26. K.Z. Stanek, et al. *ApJ* **591**, L17 (2003).
J. Hjorth, et al. *Nature* **423**, 847 (2003).
27. M. Della Valle et al. *A&A* **406**, L33 (2003).
28. H.E. Bond, et al. *Nature* **422**, 425 (2003).
29. S. Corbel, et al., *Science* **298**, 196 (2002).
30. R. D. Preece et al. *ApJS* **129**, 19 (2000).
31. L. Amati et al. *A&A* **390**, 81 (2002).
32. D. Band et al. *ApJ* **413**, 290 (1993).
33. J. K. Frederiksen et al. *ApJ* **608**, L13 (2004).
34. P. Grandi et al., *ApJ* **586**, 123 (2003).
35. I. S. Shklovskii, *Dokl. Akad. Nauk. USSR* **91**, 475 (1953).
36. P. Courdec, *Annales d'Astrophysique* **2**, 271 (1939).
37. G.B. Taylor et al., astro-ph/0405300
38. D. A. Frail et al. astro-ph/0408002.
39. T. Matheson, et al., *ApJ* **599**, 394 (2003).
40. S. Dado, A. Dar and A. De Rújula, astro-ph/0402374.
41. S. Dado, A. Dar and A. De Rújula, astro-ph/0406325.
42. D.J. Thompson and C. E. Fichtel, *A&A* **109**, 352 (1982).
43. P. Sreekumar et al., *ApJ* **494**, 523 (1998).
44. G. Bignami et al., *ApJ* **232**, 649 (1979).
45. D. N. Page and S. W. Hawking, *ApJ* **206**, 1 (1976).
46. A. Dar, A. De Rújula and N., Antoniou, astro-ph/9901004.
47. P. Ferrando et al., *A&A* **316**, 528 (1996).
48. S.P. Swordy et al., *ApJ* **330**, 625 (1990).
49. M. S. Longair, *High energy astrophysics* (Cambridge Univ. Press, 1981).
50. L. O'C. Drury, W.J. Markiewicz, and H. J. Völk, *A&A* **225**, 179 (1989).
51. A. Dar and A. De Rújula, *ApJ* **547**, L33 (2001).
52. R. Plaga, *A&A* **330**, 833 (1998).
53. L. L. Cowie and J. J. Binney, *ApJ* **215**, 723 (1997).
A. C. Fabian, *Galaxy Evolution*, Eds. V. Avila-Reese et al. (astro-ph/0210150).
54. T. Tamura, et al. *A&A* **365**, L87 (2001).
55. B. Wiebel-Sooth and P. L. Biermann, *Landolt-Börnstein*, (Springer, Heidelberg 1998).
56. A. Haungs et al., *Acta Physica Polonica* **B35**, 331 (2004).
57. D. J. Bird et al., *ApJ* **424**, 491 (1994).
58. K. Greisen, *PRL* **16**, 748 (1966).
59. G. T. Zatsepin and V. A. Kuz'min, *JETP. Lett.* **4**, 78 (1966).
59. S. Dado, A. Dar and A. De Rújula, *ApJ* **585**, 890 (2003).